Electrochimica Acta 470 (2023) 143281

Contents lists available at ScienceDirect

Electrochimica Acta

journal homepage: www.journals.elsevier.com/electrochimica-acta

Analysis of the electrochemical performance of carbon felt electrodes for vanadium redox flow batteries

José E. Barranco [a,*], Abdenbi Cherkaoui [a], Manuel Montiel [a,b], Ana González-Espinosa [a], Antonio Lozano [a], Félix Barreras [a]

[a] Instituto de Carboquímica, CSIC. Miguel Luesma Castán 4, Zaragoza 50018, Spain
[b] Fundación Agencia Aragonesa para la Investigación y el Desarrollo (ARAID). Avda. de Ranillas, 1-D, Zaragoza 50018, Spain

ARTICLE INFO

Keywords:
Electrochemical impedance spectroscopy
Felt electrodes
Redox flow battery
Vanadium
X-ray photoelectron spectroscopy

ABSTRACT

In the present research, the performance of three commercial graphite felts (a 6 mm thick Rayon-based Sigracell®, a 4.6 mm thick PAN-based Sigracell®, and a 6 mm thick PAN-based AvCarb®) used as electrodes in vanadium redox flow batteries (VRFBs) is analyzed before and after thermal activation. The thermal treatment of the electrodes at 500 °C for 1 h in a self-designed industrial furnace under a synthetic air atmosphere. XPS confirms that thermal activation provides with different C=O/C—O and sp^2/sp^3 ratios to the graphite electrodes depending on their carbon precursors, providing different catalitic behavior. T-GFD4.6-EA felt electrode was also oxidized by cycling in H_2SO_4 and in 0.4 M $VOSO_4$ + 2 M H_2SO_4 solution. In the first case, the graphite electrode increased the current density 24.27 mA cm^{-2} for the VO^{2+} electrooxidation, however the cathodic current density (VO_2^+ reduction reaction) was decreased 36 mA cm^{-2}. In the second case, the increase was of 21.27 mA cm^{-2}, whereas the current density for the VO_2^+ reduction hardly changed. Thermally treated GFD4.6-EA graphite felt chemical composition also changed differently when exposed to different laboratory experiments which mimic the electrode behavior in a VRFB. XPS analysis confirmed that the chemical modification of the graphite surfaces can either improve or decrease the electrocatalytic activity of the electrodes depending on their carbon precursors.

1. Introduction

Nowadays renewable energy sources are receiving a great boost due to climatic change and geopolitical strategies. Among them, solar and wind are the most promising resources to develop renewable energy systems to reach this goal in Spain. However, intermittency in the energy production due to seasonality and the, sometimes, low quality electrical signal due to fluctuations in both frequency and voltage, force the integration of different technologies to store the excess energy in order to increase the network stability with renewable energy systems. All-vanadium redox flow batteries (VRFBs) are a promising large-scale energy storage technology. These devices have a large cyclability that means a very long lifetime, and their power and capacity range can be sized independently, which is very relevant for stationary applications [1].

Although the stack in RFBs comprises membranes, current collectors and bipolar plates, the electrocatalytic reaction occurs at the electrodes. Thus, the appropriate selection of the electrode material is crucial for the overall battery performance because it has a great impact on the activation overpotentials, electrochemistry polarization as well as on the Ohmic and concentration polarization. Due to their high surface area, mechanical stability and catalytic sites availability, the most common electrodes used for VRFBs are the carbon felts, specifically, those formed by carbonized (CF) or graphitized (GF) Rayon (cellulose) and PAN (polyacrylonitrile) fibers [2]. These felts exhibit a relative low activity towards redox reactions in VRFBs and poor wettability. For these reasons, it is necessary to improve their physicochemical properties. Such improvements may include surface modification by plasma treatment to increase the wettability by the formation of both, deep and surface oxygen functional groups, thus improving the energy efficiency of the VRFB [3]. Other different techniques are aimed to increase the surface area by adding multiwalled carbon nanotubes (MWCNTs), carbon nanoparticle [4,5] and metallic modifications [6,7]. In some research works chemical and electrochemical oxidation treatments are used to improve the performance of the electrodes [2]. Conducting polymers such as polypirrole (PPy), polyaniline (PANI), and polyacetylene (Pac), among others, have also been used to modify CF electrodes in the energy

* Corresponding author.
E-mail address: j.barranco@csic.es (J.E. Barranco).

https://doi.org/10.1016/j.electacta.2023.143281
Received 20 December 2022; Received in revised form 24 July 2023; Accepted 29 September 2023
Available online 30 September 2023

Nomenclature

Latin letters

A	electrode area [cm^2]
C	concentration [mol L^{-1}]
CE	counter electrode
CF	carbonized fiber
CPE1	constant phase element
CV	cyclic voltammetry
D	diffusion coefficient [cm^2 s^{-1}]
EE	energy efficiency
EIS	Electrochemical Impedance Spectroscopy
F	Faraday constant (96,485 C mol^{-1})
GF	graphitized fiber
AVCARB6	6 mm thick PAN-based AvCarb® graphite felt
GFD4.6-EA	4.6 mm thick PAN-based Sigracell® graphite felt
GFA6-EA	6 mm thick Rayon-based Sigracell® graphite felt
I_p	maximum current [A]
j	current density [A cm^{-2}]
j_0	exchange current density [A cm^{-2}]
LSV	Linear Sweep Voltammetry
MIP	mercury intrusion porosimetry
n	number of electrons
NT	nominal thickness [m]
OCP	open circuit potential [V]
OP	open porosity [m]
T-AvCarb6	AVCARB6 graphite felt thermally treated
T-GFD4.6	GFD4.6-EA graphite felt thermally treated
T-GFA6	GFA6-EA graphite felt thermally treated
PAN	polyacrylonitrile fiber
PD	pore diameter [m]
PPT	potentiostatic polarization treatment
PV	pore volume [m^3]
R	universal gas constant (8.3145 J K^{-1} mol^{-1})
R1	contact resistance of the solution [mΩ·cm^2]
R2	transfer resistance at the electrode-electrolyte interface [mΩ·cm^2]
RE	reference electrode
SD	skeletal or real density
SSA	specific surface area
T	absolute temperature [K]
V	scan rate [mV·s^{-1}]
VRFB	all-vanadium redox flow battery
WE	working electrode
Ws1	Warburg element
XPS	X-ray photoelectron spectroscopy

Greek letters

α	symmetry factor
η	overpotential [V]

research area [8,9]. Li et al. [10] studied the performance of graphite felt electrodes (GF) modified with PPy conducting polymer. They found an optimal catalyst load at which the modified graphite felts, GC, exhibited higher discharge capacity and energy efficiency (EE) compared to air treated GF electrodes at 80 mA·cm^{-2}. Also, these modifications enhanced the electrochemical activity, reversibility and cycling stability of the GC when tested in a vanadium redox flow single cell. Eifert et al. [11] studied the effect that thermal treatment, soaking and electrochemical aging have on commercial PAN and Rayon-based carbon felt electrodes. They found that the different treatments used had different effects on the carbon felts depending on the precursor used to manufacture them and the pre-treatment (carbonization or graphitization) employed. For instance, it was shown that the thermal stability after thermal treatment was lower for carbonized felts compared to graphitized felts and that the Rayon based felts were more stable than the PAN-based ones. Soaking was shown to have higher impact on the thermal stability of PAN-based carbon felts, and on the electrochemically aged Rayon ones. Thermal oxidation stands out as one of the more used and easier ways to generate high functionalized and enhanced active surface area in carbon felt electrodes by the incorporation of oxygen functional groups. However, the thermal treatment needs to be optimized in time duration and temperature. Kaur et al. [12] studied the stability of the CF electrodes after thermal treatment analyzing their mechanical properties when subjected to compression tests (from 0 to 70 % compression). They found that longer thermal treatments modify the mechanical properties due to the release of CO_2 from the surface and the consequent pore formation. Temperatures above 600 °C showed significant mass reduction at short time intervals. This reduction had a direct impact on the pressure needed to achieve the same compression ratios as those for the CF treated at lower temperatures.

In this study, the influence of thermal treatment and electrochemical aging of commercial GF materials (PAN and Rayon-based) on their electrochemical properties is studied in order to properly select a reliable electrode for a particular VRFB system design. Surface chemistry of the GF electrodes was investigated by X-ray photoelectron spectroscopy (XPS). Porous grade was checked by mercury porosimetry and compared with the results obtained by Electrochemical Impedance Spectroscopy (EIS). Electrochemical characterization tests were carried out in a three-electrode configuration electrochemical reactor using cyclic voltammetry and EIS techniques.

2. Experimental

2.1. Electrode material and activation

Three commercial graphite felt electrode materials are used in this research: a Rayon-based Sigracell® GFA6-EA (6 mm thick) thermally treated (identified as T-GFA6), a PAN-based Sigracell® GFD4.6-EA (4.6 mm thick) electrode, thermally (T-GFD4.6) and non-thermally treated (GFD4.6), and a PAN-based AvCarb® AVCARB6 (6 mm thick) thermally treated (T-AvCarb6). The 6 mm thick GF electrodes were manufactured bonding two 3 mm thick felts together. The maximum compression tolerance of the electrodes, according to the manufacturers is 50 % and 30 % for the 6 mm and 4.6 mm thickness, respectively.

Due to the fiber arrangement and the high porosity, the electrode material is soft and compressible, ideal to be used in redox flow batteries. The T-GFA6, T-GFD4.6 and T-AvCarb6 felt electrodes were subjected to a thermal treatment that consisted in keeping the electrodes at 500 °C for 1 h in a self-designed industrial furnace under a synthetic air atmosphere to introduce active sites on the carbon surface and to enhance their wettability [13,14]. Activation of T-GFD4.6 surface electrodes was carried out by immersion in a beaker containing 2 M H_2SO_4 + 0.4 M $VOSO_4$ electrolyte at 30 °C for 5 days and by means of cyclic voltammetry cycling the samples 100 times at 50 mV s^{-1} for voltages ranging between 0 V and 1.4 V.

2.2. Electrolyte preparation

Two solutions have been prepared: one 2 M H_2SO_4, used for EIS characterization of the different electrodes previous to any polarization activation; and the vanadium electrolyte prepared dissolving 0.4 M VOSO4 ·5 H2O (chemically pure, Sigma Aldrich®) in 2 M H_2SO_4 (97 % purity, PanReac AppliChem®) to study the effect of the thermal pretreatment, immersion effect and polarization aging on the activity of

the graphite electrodes.

2.3. Electrode characterization

The electrochemical activity of the GF electrodes was characterized by Cyclic Voltammetry (CV), Linear Sweep Voltammetry (LSV) and Electrochemical Impedance Spectroscopy (EIS). The tests were performed in a classical three electrode configuration in a 125 cm^3 thermostated (25 °C) reactor, Fig. S1. A platinum sheet was used as counter electrode (CE), and an Ag/AgCl, 3.5 M KCl (i.e., 0.209 V vs. NHE) electrode as the reference one (RE). This RE was immersed in the solution through a Lugging capillary, which defined a clear sensing point for the reference electrode kept at a constant distance of 1 mm from the working electrode (WE). The different graphite felts (5.71 cm^2 geometric surface area) were used as WE, and were electrically connected inserting a platinum wire. All the WEs were previously wetted with the different solutions using a syringe at very low pressure. This strategy avoided the formation of bubbles and eased the internal wetting of the electrodes when immersed into the solutions.

All the electrochemical analyses were performed using an Autolab PGSTAT302N combined with a FRA32M module. Cyclic voltammetry experiments were performed in a 0.4 M VO^{2+} + 2 M H_2SO_4 unstirred solution at a scan rate of 10 mV s^{-1} for a potential ranging from 0 to 1.4 V vs Ag/AgCl 3.5 M KCl. A similar procedure was used to accomplish the linear sweep voltammetry tests, but using an output potential difference range from 0.3 to 0.9 V vs Ag/AgCl 3.5 M KCl.

Concerning the EIS analysis, all the experiments were performed using the FRA32M module of the PGSTAT302N workstation using the same electrolyte as in the CV, at a polarization potential of 1.009 V (vs. Ag/AgCl) and an amplitude of 10 mV over a frequency range from 10 Hz up to 100 kHz. Before the electrode aging procedure was started, the electrodes were characterized by EIS in a 2 M H_2SO_4 solution. For each sample, the open circuit potential (OCP) was recorded for 15 min in order reach steady conditions. Then, all the tested electrodes were exposed to an aging procedure using a potentiostatic polarization treatment (PPT) at 1.6 V vs Ag/AgCl 3.5 M KCl in low-concentrated vanadium-acid electrolyte (0.4 M $VOSO_4$ + 2 M H_2SO_4). With this potential value in such oxidative electrolyte, the high stress on graphite materials is ensured [6] so that results could be obtained in a shorter time.

2.4. XPS characterization

X-ray photoelectron spectroscopy (ESCAPlus Omicron System) in a test area of 1.75 × 1.75 mm^2 has been used to study the elemental and chemical state of the samples and thus, to elucidate the effects that the aging treatment had on their graphitized surfaces. Measurements were performed using a monochromatic Al Kα anode radiation (300 W, 15 kV) with pass energies of 50 and 20 eV to the electron energy analyzer for both survey and high-resolution spectra, respectively. The detection angle was 45°, and the samples were previously dried at 110 °C in a vacuum oven for 1.5 h.

2.5. Mercury porosimetry

Mercury intrusion porosimetry (MIP) has been used to evaluate the porosity, pore size distribution, and pore volume of the GF samples. Measurements have been performed in a MicroActive AutoPore V 9600 Version mercury intrusion porosimeter from Micromeritics using a maximum pressure of 33 000 psia (2 275 bar). Prior to analysis, samples were vacuumed dried at 110 °C for 4 h to eliminate humidity and other gasses adsorbed in the porous structure. Cumulative specific volume measurements were collected in both intrusion and extrusion modes. To perform the measurements, a single piece of felt of approximate 1–1.5 cm^2 was used. The mercury parameters used in the analysis configuration of the MicroActive software were: a surface tension of 480 erg cm^{-2} and a contact angle of 130°. Porosity values were calculated for the bulk density of the sample at 1 psia (0.06874 bar), considering that the intraparticle filling starts at that point according to the Washburn formulation [15].

It is important to be noted that MIP requires specialized equipment and special safeties need to be taken to ensure the proper handling of mercury. Thus, if the physical and chemical characteristics of the porous material and the expected pore size distribution allows it, the non-adsorbable gas porosimetry could be an alternative experimental technique.

3. Results and discussion

The positive VO^{2+}/VO_2^+ reaction involves complex multistep processes and has sluggish kinetics compared to the negative reaction. already observed by Gattrell et al. [16,17]. The effect of the thermal treatment on the GF has been widely studied. It is agreed that it incorporates surface-active oxygen functional groups which catalyze the VO^{2+}/VO_2^+ redox reactions. Nevertheless, these electrodes are also superficially modified when they are used in real redox flow batteries. Actually, the performance of the thermally modified electrodes can be modified again by the cycling process, the oxidative character of the electrolyte, the temperature, and the potential limits of the operational battery. In this study all the used samples were thermally pre-treated using a self-designed industrial furnace under an air atmosphere. The different thermally treated electrodes are physical and electrochemically compared to the untreated ones. Also, the influence of cycling and immersion of the thermally pre-treated electrodes on the surface modification is studied trying to replicate the aging of such electrodes when performing in a real vanadium redox flow battery.

3.1. Physical-chemical characterization

Proper selection of the electrode material is crucial for the overall performance of the battery because it has a great impact on the activation overpotentials, electrochemical polarization, as well as in both ohmic and concentration polarization [18–21]. all three felt electrodes (T-AvCarb6, T-GFD4.6 EA, and T-GFA6 EA) have porous structures with interconnected carbon fibers.

However, the way the interconnections of the carbon fibers are made appears to be one of the main differences between the Sigracell and the AvCarb electrodes. All Sigracell electrodes showed a clear interwoven of carbon fiber well oriented whereas the AvCarb shows a compaction-like interconnection of the carbon fibers with no interwoven and preferential orientation. Fig. 1 shows the photographs of the electrode samples used in this study where the yellow lines shows the fibers orientation observed in the Sigracell electrodes. Moreover, T-AvCarb6 electrode showed a softer morphology compared to the other Sigracell electrodes, without a clear interwoven of its fibers, which may cause rapid deterioration. Moreover, high compression of this electrode resulted in a crumbling of its physical structure, which was not observed in the other electrodes. Table 1 summarizes the results of MIP measurements to determine the open porosity (*OP*), the pore volume (*PV*), the average pore diameter (*PD*), the specific surface area (*SSA*) and the skeletal or real density (*SD*), which represents the ratio of the mass of solid material to the sum of the volumes of the solid material and closed pores within the GF samples. In the table, the nominal thickness (*NT*) and the precursors of the GF according to the manufacturer specifications are also shown.

All samples showed a unimodal pore distribution centered between 50 and 60 μm, which corresponds to the macroscopic voids in the felts as depicted in Fig. 2. T-AvCarb6 appears to be the least porous material with a pore size range between 36 and 92 μm, representing 64 % of the total pore volume (4.2 mL g^{-1} over 6.6 mL g^{-1}).

The pore size distribution shows a low differential intrusion for the pore size range between 16 and 30 μm for all the samples. These values

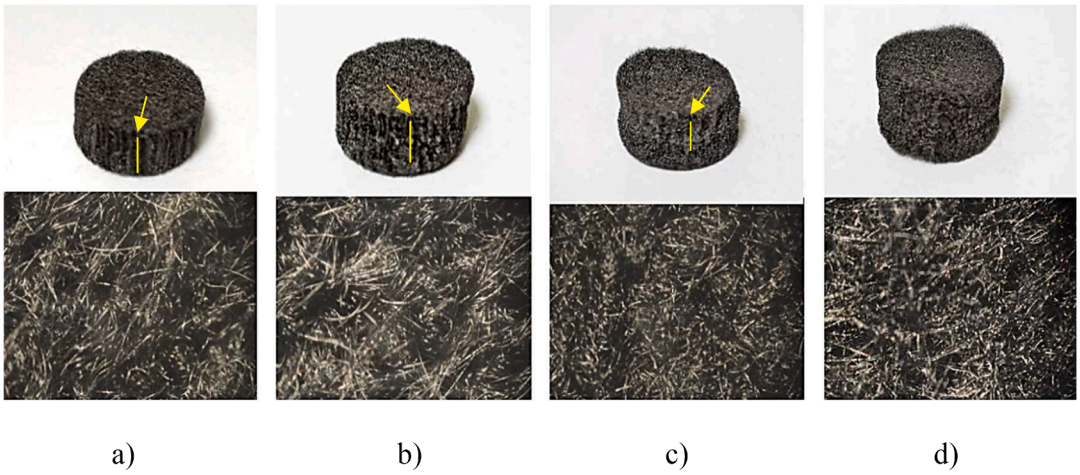

Fig. 1. Photographs of the electrodes used: (a) GFD4.6 (PAN), (b) T-GFA6 (Rayon), (c) T-GFD4.6 (PAN) and (d) T-AvCarb6 (PAN). Yellow lines shows the visible vertical orientation of the interweaved graphite fibers, not appreciable for the T-AvCarb6 (PAN) electrode. Lower images shows the top surface of the felts.

Table 1
Summary of sample properties obtained by MIP.

Carbon felt	Precursor	Pre-treatment	*NT* [mm]	*PV* [mL/g]	*SSA* [m^2/g]	*OP* [%]	*PD* [μm]	*SD* [g/mL]
T-GFA6	Rayon	Graphitized	6.0	9.43	0.71	91.70	53.27	1.19
GFD4.6-EA	PAN	Graphitized	4.6	8.07	0.53	91.90	61.44	1.41
T-GFD4.6	PAN	Graphitized	4.6	6.54	0.49	91.74	52.78	1.70
T-AvCarb6	PAN	Graphitized	6.1	6.61	0.56	91.90	47.27	1.72

T-GFA6 and T-GFD4.6 show values of 71 % and 72 % of the total pore volume (between 36 and 92 μm per size for both electrodes) which corresponds to 6.6 mL g^{-1} over 9.4 mL g^{-1}, and 4.7 mL g^{-1} over 6.5 mL g^{-1}, respectively. GFD4.6-EA presents the most porous structure, with 85 % of the total pore volume, which corresponds to 6.8 mL g^{-1} over 8 mL g^{-1}.

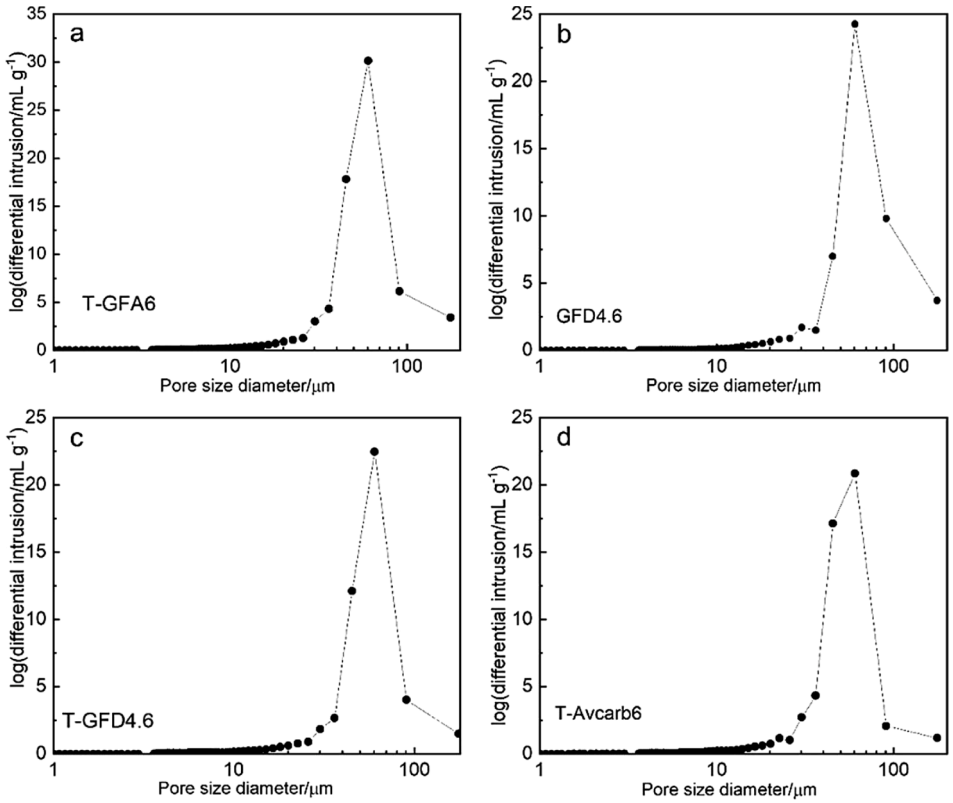

Fig. 2. Pore size distribution of (a) T-GFA6, (b) GFD4.6-EA, (c) T-GFD4.6 and (d) T-AvCarb6 electrodes obtained by Mercury Intrusion Porosimetry.

could be associated to the existing voids of the bundled fibers. As shown in Fig. 1, except for the T-AvCarb6 where the fibers are chaotically arranged, the morphology of the other felts shows interweaved graphite fibers. The bulk part of the *PV* related to the interfiber voids are 0.13 mL g^{-1}, 0.14 mL g^{-1}, 0.24 mL g^{-1} and 0.27 mL g^{-1} for GFD4.6-EA, T-GFD4.6, T-AvCarb6 and T-GFA6, respectively. It is also remarkable the low SSA values measured, suggesting a low porosity of the fibers for all the samples. This can also demonstrate the existence of pore diameters below 3 μm (interfiber voids) that cannot be detected by the MIP technique.

Concerning the heat treatment, it was not observed a great effect on the OP of the samples. However, the high bulk density value (0.14 g mL^{-1}) obtained for the T-GFD4.6 compared to the one for the GFD4.6-EA (0.11 g mL^{-1}) indicates that the thermal treatment may untangle the inter-fibers, or increase the fibers defects due to the CO_2 evolution caused by the reaction of carbon and oxygen [12], creating new micropores in the graphite structure. This would explain the increase in the skeletal or real density while the measured pore volume and the pore diameter decreases. *SSA* values for the T-GFD4.6 are similar to the value for the GFD4.6-EA, which can be explained by the pore size detection limit of the MIP technique.

The increase in the catalytic activity of the carbon felts for the electrochemical oxidation of VO^{2+} to VO_2^+ is related to the concentration of oxygen functional groups in the surface of the samples. Thus, in order to obtain direct information of the elementary composition of the GF surface and to elucidate the effects of the treatment methods on the surface composition, the samples were characterized by XPS. The type of bonding and the functional groups in the samples were estimated by deconvolution of the C1s spectra, obtained from the high-resolution spectra, using a Gaussian–Lorentzian peak shape, after performing a Shirley background correction. To compare the effects of the different treatments on the electrode surface, C/O, sp^3/sp^2 and C=O/C-O ratios were also calculated. In this sense, the C/O ratio was obtained from the atomic composition of the survey XPS spectra, the sp^3/sp^2 ratio was calculated using the deconvoluted C1s spectra and the C=O/C-O ratio was obtained from the O1s deconvoluted spectra (Table 2). To perform the analysis, different components need to be defined. In relation to the C1s components, they can be assigned as follows [22,23]: graphite carbon C=C (284.1 eV), C—H or C—C (284.5 eV; 0.3 to 0.5 eV with respect to C=C), C—O-R (285.2 eV; 1.8 to 2.2 eV), C=O (288.2 eV; 3.3 to 3.5 eV), HO—C=O (290.2 eV; 4.3 to 4.8 eV) as shown in Fig. 3.

More relevant information about the nature of the surface composition was obtained by the O1s and N1s XPS fitted from the high-resolution spectra, which comprises the following chemical states: C=O (531.4 eV ± 0.3 eV), C—O (532.7 eV ± 0.3 eV), and -O- from hydroxyl or carboxyl groups (534.3 eV ± 0.3 eV), as can be observed in Fig. 4. For T-GFA6, when the graphite was modified the following O1s deconvolution for the chemical states [20] was reported: C—O (532.3 eV), C=O (533.3 eV) and the -O- anhydride-pyrone.

The N1s peaks appeared for the samples after different activation methods (Fig. S3 of the supplementary information). Pyrrolic-N with electronic state (399.98 eV) appeared for T-GFD4.6 activated after 100 CV cycles in 2 M H_2SO_4, as well as nitrogen for the T-GFD4.6 electrode after being immersed in 2 M H_2SO_4 + 0.4 M $VOSO_4$ electrolyte during 5 days. This peak can be resolved into two species: pyrrolic-N (399.94 eV ± 0.1 eV, 48.95%) and pyridinic-N (398.4 eV ± 0.1 eV, 8.28%) [24,25]. The rest of the C1s and O1s spectra together with the N1s are shown in the supplementary material (Figs. S2–S4) with the related peak values in Tables S1–S3.

Table 2
Total surface chemical composition of the samples from the survey spectra.

Samples	O%	C%	N%	O/C ratio
GFD4.6-EA	0.83	99.17		0.01
T-GFD4.6 (immersion 2 M H_2SO_4 + 0.4 M $VOSO_4$)	5.92	92.11	1.97	0.06
T-GFD4.6	3.76	96.24		0.04
T-GFD4.6 (100 CV cycles 2 M H_2SO_4 + 0.4 M $VOSO_4$)	2.37	97.63		0.02
T-AvCarb6	3.21	96.79		0.03
T-GFA6	3.59	96.41		0.04
T-GFD4.6 (100 CV cycles in 2 M H_2SO_4)	16.05	81.86	2.09	0.20

According to the obtained results, and looking at Table 2, the total oxygen content is increased when the GFD4.6-EA electrode is thermally treated. To elucidate which oxygenated species is mainly formed on the basal graphite plane Fig. 3 shows a 16 % increase in the C—O-R peak (285.2 eV) of the thermally treated Sigracell carbon felt (T- GFD4.6) compared to the untreated one (GFD4.6-EA). This is also shown in the supplementary information (Table S1). It can be seen that there is a small increase of the C—O-R concentration, and a notorious formation of the C=O carbon species. Moreover, although the sp^2/sp^3 ratio is reduced by 3.9 %, the C=O/C—O ratio increases by 204 %. This means that the thermal treatment for this electrode incorporates more oxygen which mainly bonds to sp^2 carbons stimulating the formation of C=O, but hydroxyl carboxyl species are also formed. This can enhance the conductivity of the electrode when oxidizing the vanadium ions. Thermal pre-treatment also reduces the concentration of C—H bonds, which do not take part in the redox reaction but enhance the number of defects on the graphite surfaces.

Some differences in the thermal treatment effects on T-AvCarb6 compared to T-GFD4.6 (both graphite electrodes with PAN precursor) were also found. As shown in Table 2, there is a slight decrease in the total oxygen content for the former GF. The C=O/C—O ratio clearly decrease compared to the latter GF electrode, which is attributed to the formation of hydroxyl or carboxyl compound. This behavior may ease the reversibility in the electro-oxidation of the VO^{2+}/VO_2^+ redox couple. Additionally, although the oxygen content is lowered, most of the oxygen is bonded to sp3-carbon in the form of C—O compounds, as can be seen in Tables S1 and S2 of the supplementary material. The 6.50 % decrease in the C=O/C—O ratio for the T-AvCarb6 electrode with respect to the one found for the T-GFD4.6 electrode allows to ensure that the former electrode will have better conductivity and better reversibility than the last one. The higher C—O, C=C and H—C=O functional group concentration supports such prediction. Moreover, as will be seen lines below, cyclic voltammetry experiments also corroborate this conclusion.

Aging of the already thermally treated T-GFD4.6 electrodes after 100 cycles using the cyclic voltammetry technique and by immersion, affects the electrode surface in a different way. When the electrode was immersed in the 2 M H_2SO_4+ 0.4 M $VOSO_4$ electrolyte at 30 °C for 5 days, the O/C ratio increased by 50 %, on the contrary, the O/C ratio decreased by 50 % when cycled in the same electrolyte. Such an increase is due to the higher oxygen content which clearly appears in the form of C=O functional groups, more precisely in the form of HO—C=O functional group, increasing the sp^2/sp^3 ratio by 27 % and the C=O/C—O ratio by 67 %. Apparently, the reversibility of the sample should be reduced, according to the previous analysis, but another factor needs to be considered. As seen in Tables 2 and S3, the immersion process creates N1s compounds in the surface of the electrode, which favors catalytic activity for the graphite samples [26]. So, activation by immersion in the vanadium solution increases the number and type of functional groups in the electrode surface, helping the catalysis of the VO^{2+}/VO_2^+ oxidation reaction. It is accepted that the COOH group provides H^+ more easily than the C—OH [27]. Also, C=C functional groups are slightly increased, which is related to the double layer capacity enhancement, due to electrochemical oxidation and roughening when immersed in the electrolyte [11].

3.2. Electrochemical characterization

In order to quantify the improvement of the electrochemical activity

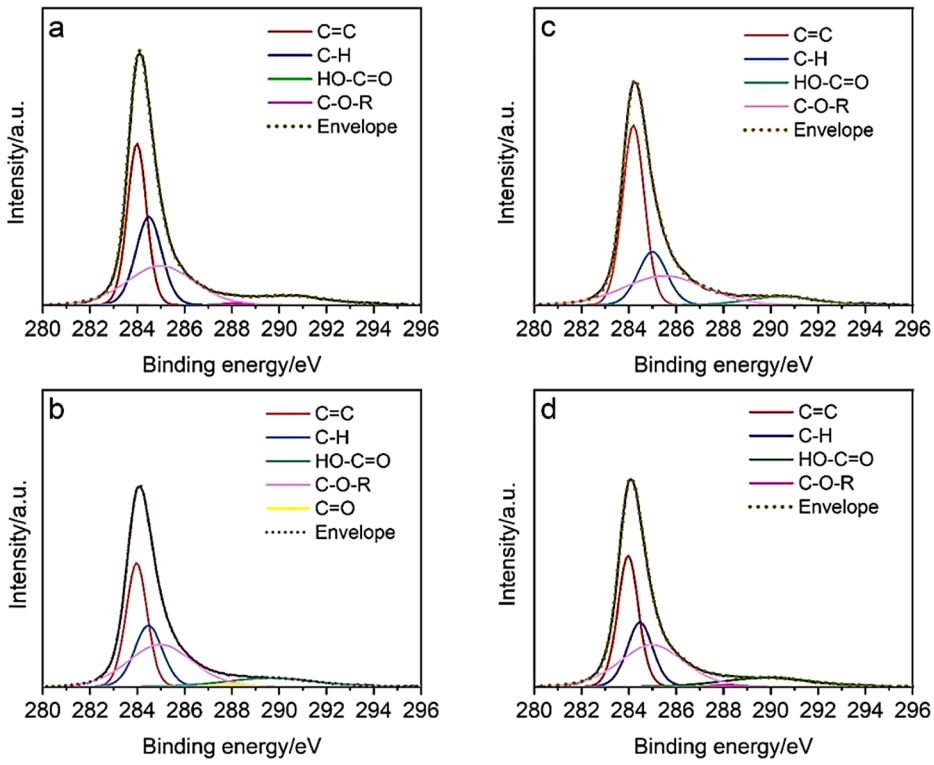

Fig. 3. Deconvoluted XPS spectra of the C1s for (a) GFD4.6-EA, (b) T-GFD4.6, (c) T-GFA6 and (d) T-AvCarb6.

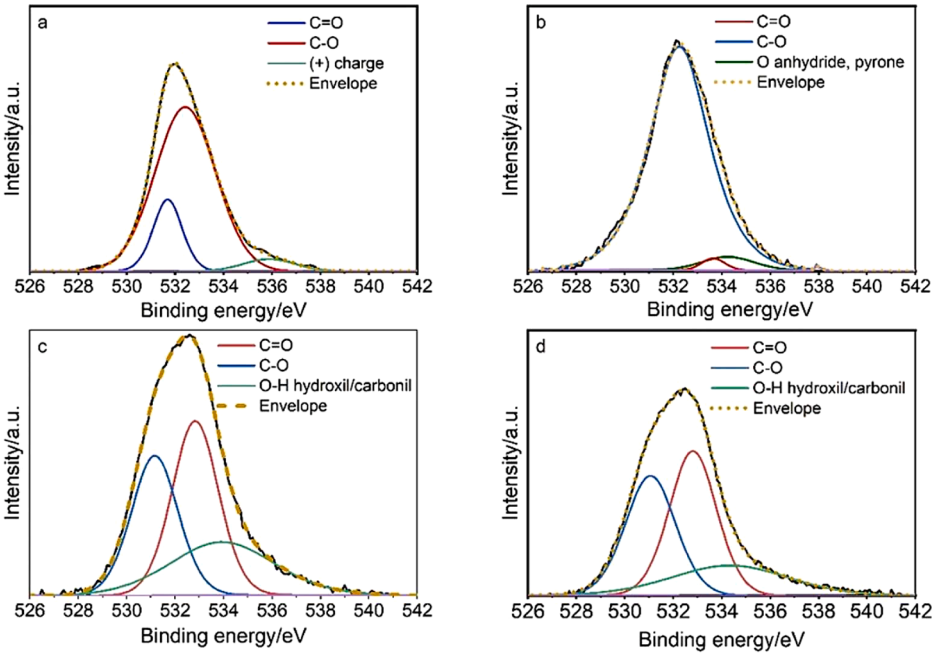

Fig. 4. Deconvoluted XPS spectra of the O1s for (a) GFD4.6, (b) T-GFD4.6, (c) T-GFA6 and (d) T-AvCarb6.

of the graphite felts after the thermal treatment, and to determine the corresponding kinetic parameters, linear sweep voltammetry and cyclic voltammetry are performed to the untreated electrodes (GFD4.6-EA and GFA6) and to the thermally treated ones (T-GFA6, T-GFD4.6 and T-AvCarb6). The potential window was set to 0.3–0.8 V vs Ag/AgCl, 3.5 M KCl as reference electrode in the 2 M H_2SO_4 + 0.4 M $VOSO_4$ electrolyte. A 2 cm^2 platinum foil was used as counter electrode and the scan rate was set to 10 mV s^{-1}. Fig. 5 clearly indicates, by the shift of the onset potential towards more negative values, that the thermal treatment has positive effects on the kinetics of the electro-oxidation reaction of the VO^{2+}/VO_2^+ species.

The thermal treatment decreased the onset potential from which faradaic processes take place by 280 mV, 240 mV and 80 mV for T-GFD4.6, GFA6-EA and AvCarb6, respectively. It can, then, be inferred that the thermal treatment has a major impact on the GFD4.6 felt electrode when it is compared to the untreated samples. It is noteworthy, however, that the T-GFA6 electrode reached the higher current density at 0.8 V, compared to the other 6 mm thick electrode AvCarb6.

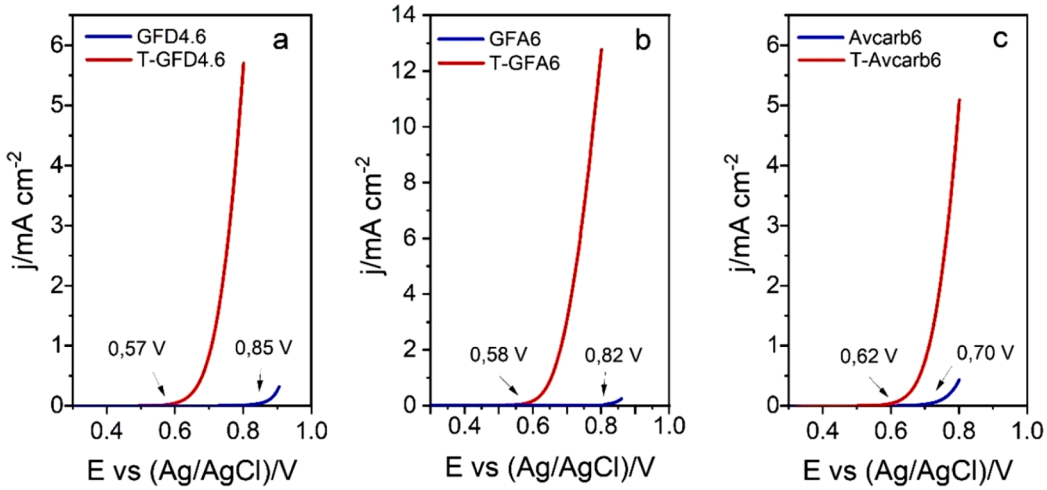

Fig. 5. Linear Sweep Voltammetry of (a) GFD4.6-EA, (b) GFA6 and (c) Avcarb6. Untreated electrodes (blue) and the thermally treated ones (red).

Analysis of the logarithms of the current density against overpotential in the electronic transfer limited region, Fig. S5a-b, allows to determine some important kinetic parameters.

Using the Tafel equation:

$$Ln|j| = Ln|j_0| - \frac{\alpha F \eta}{RT} \quad (1)$$

where *j, j_0, α, F, η, R* and *T* are the current density, the exchange current density, the symmetry factor, the Faraday constant, the overpotential, the universal gas constant and the absolute temperature, respectively. From the j_0 values we can see that most oxidation processes are favored for the thermally treated electrodes compared to the untreated ones, as can be observed in Table 3. Moreover, the higher exchange current densities values (from 1 up to 2 orders of magnitude in the case of AvCarb6), together with the values of the symmetry factors, close to 0.5 for the thermally treated samples, also indicate that the thermal treatment has positive effects on the kinetics of the VO^{2+}/VO_2^+ electro-oxidation reaction and that the current has a symmetrical contribution from both, the reductive and oxidative reactions.

Cyclic voltammetry is another electrochemical technique used to characterize the electrodes. In Fig. 6a, voltammograms for the commercial T-GDF4.6 electrode before and after 100 CV activation cycles at 50 mV s^{-1} between 0 V and 1.4 V in the 2 M H_2SO_4 + 0.4 M $VOSO_4$ electrolyte are shown. It can be observed that the potential difference, ΔE, between the anodic and cathodic peaks obtained for the cycled electrode is 0.8 V, about 26 % of reduction if compared to the one not cycling activated. Moreover, it can be observed that the anodic current density increases up to 129.4 mA cm^{-2} (at 1.29 V) after the cycling activation, whereas the cathodic one decreases to −60 mA cm^{-2} current density value (at 0.49 V). This decrease means a current density difference of 35 mA cm^{-2} compared to the T-GDF4.6 electrode before the cycling activation. This behavior can be explained looking at Tables 2 and S1. While the total oxygen content decreases by 58.6 %, the sp^2/sp^3 and C=O/C—O ratios decrease because the oxygen at the surface after cycling mainly appears as C—O, and also, C=H increases. The result is an electrode that shows higher reversibility in the oxidation of the VO^{2+}/VO_2^+ species and a higher conductivity. To elucidate if this behavior was caused by the highly oxidative electrolyte in which the electrode was activated, and that contained 0.4 M $VOSO_4$, the 100 CV activation cycles were also accomplished in a 2 M H_2SO_4 solution (free of vanadyl salts), as depicted in Fig. 6b. Activating the T-GFD4.6 electrode in sulfuric acid causes a reduction of the cathodic current in the CV at vanadyl electrolyte, which decreases the I_{pa}/I_{pc} ratio compared to the one obtained for the sample before been cycled. With this treatment a more reversible and conductive electrode is also achieved, corroborating the increase of the C=C.

Table 3
Kinetic parameters of the thermally treated and untreated samples.

Sample	α	j_0 (A cm^{-2})/ 10^{-4}
T-GFD4.6	0.59	16.6
GFD4.6-EA	0.8	0.85
T-AvCarb6	0.59	7.1
AvCarb6	0.79	2.3
T-GFA6	0.73	165
GFA6-EA	0.27	0.08

The diffusion coefficient of the VO^{2+} ions was calculated from the Randles-Sevcik equation:

$$I_p = 2.69 \cdot 10^5 . A . D^{1/2} . n^{3/2} . V^{1/2} . C \quad (2)$$

where I_p, *n, A, D, C,* and *V*, are the maximum current, the number of electrons transferred in the redox reaction, the electrode area, the diffusion coefficient, the concentration, and the scan rate. Fig. 7, shows the cyclic voltammetry at different scan rates for the T-GFD4.6 and T-AvCarb6 electrodes in 0.4 M $VOSO_4$ + H_2SO_4 solution.

There is a deviation from unity in the anodic to cathodic peak current ratios at lower scan rates for the T-GFD4.6 electrode, as depicted in Fig. 7a, until unity is reached at 10 mV s^{-1}. However, the higher the scan rate, the higher the potential range. These two behaviors imply that the electro-oxidation reaction of the VO^{2+}/VO_2^+ species showed quasi-reversible electrochemical kinetics, but the conductivity capacity of the electrode is decreasing, probably due to limitation of the vanadium ion diffusion into the felt pores at high scan rates.

Concerning the performance of the T-AvCarb6 electrode, from the values of the peak current ratios and the potential range it can be seen that, as the potential rate increases, this electrode shows a reversible behavior towards the electrochemical oxidation of the VO^{2+}/VO_2^+ species. Moreover, the electrode tends to be activated by the cycling procedure in the vanadyl solution, which enhances its electrochemical activity. Also, as shown in Table S2 of the supplementary material, oxygen content in the form of C—O and hydroxyl species is high compared to the T-GFD4.6 electrode, which enhances the VO^{2+}/VO_2^+ oxidation reaction. As can be observed in Fig. 8, for the T-GFA6 electrode the current ratio values barely change as the scan rate is increased. However, the higher the scan rate the higher the potential range. This performance is typical of a diffusion-controlled process. In order to clarify this point, the representation of the logarithm of the cathodic peak current against the logarithm of the square of the scan rate is performed for all the thermal treated electrodes in Fig. S6. The diffusion coefficients values for the VO^{2+} ions obtained from the Randles-Sevcik equation are

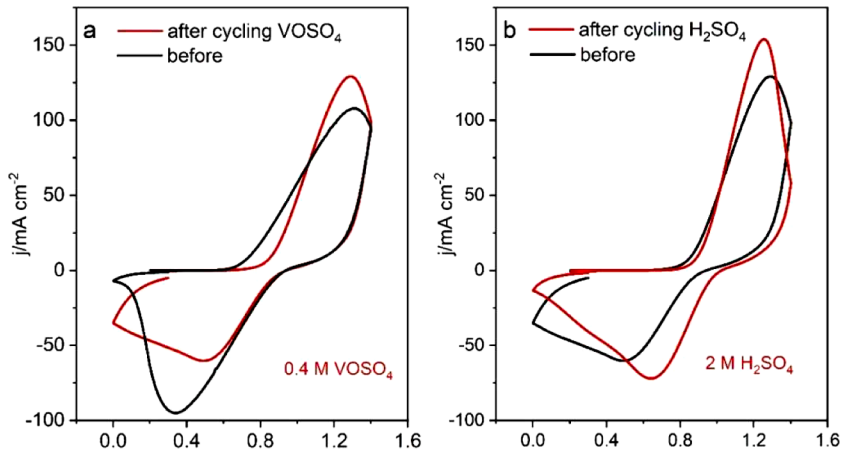

Fig. 6. Voltammograms for the commercial T-GFD4.6 electrode in 0.4 M $VOSO_4$ + 2 M H_2SO_4 electrolyte at 50 mV s^{-1} between 0 and 1.4 V (vs Ag/AgCl, 3.5 M KCl), before and after 100 cycles activation in (a) 0.4 M $VOSO_4$ + 2 M H_2SO_4, (b) H_2SO_4.

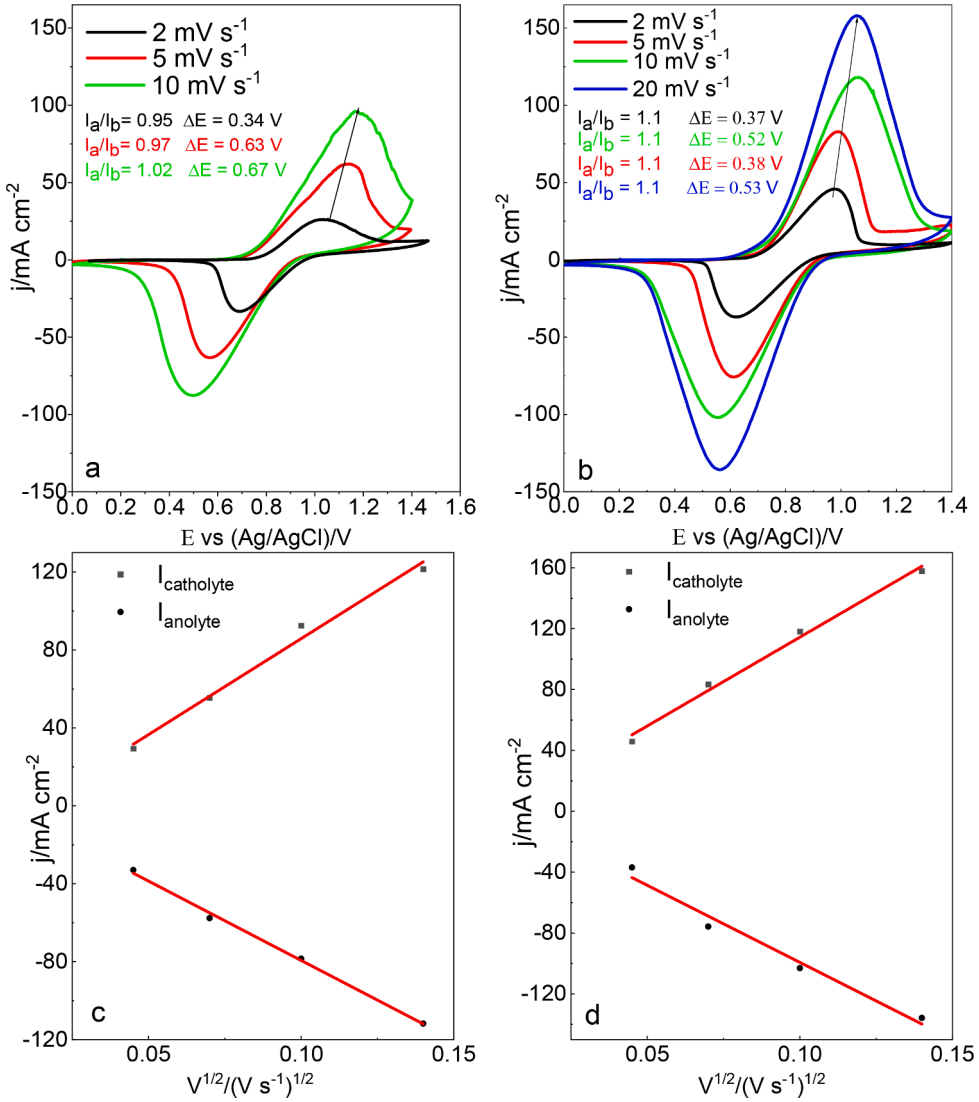

Fig. 7. Cyclic voltammetry of (a) T-GFD4.6 and (b) T-AvCarb6 electrodes at different scan rates against Ag/AgCl, 3.5 M KCl counter electrode. (c) and (d) are the fittings of I_a and I_c against the square root of the scan rate.

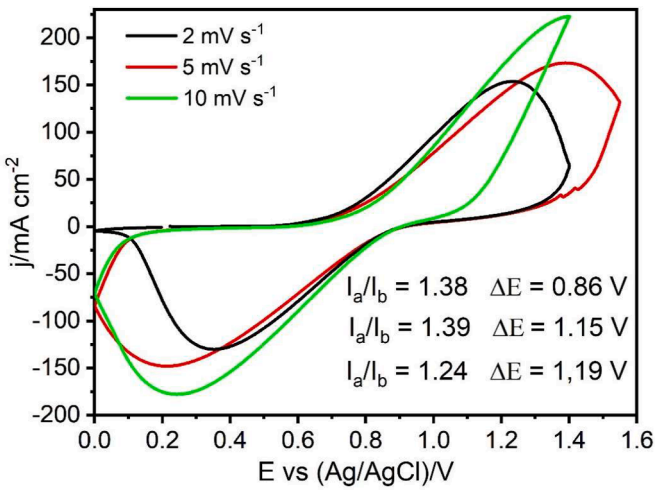

Fig. 8. Cyclic voltammetry of T-GFA6 electrode at different scan rates against Ag/AgCl, 3.5 M KCl counter electrode.

3.2×10^{-6} cm^2 s^{-1}, 4.5×10^{-6} cm^2 s^{-1} and 5.8×10^{-6} cm^2 s^{-1}, for T-GFD4.6, T-AvCarb6, and T-GFA6, respectively, in good agreement with the results reported in the literature [28,29]. Moreover, as shown in Fig. S6 for the linear relationship between the logarithm of the redox peak current and the logarithm of the scan rate for the thermal pre-treated electrodes, the slope is close to 0.5 for T-AvCarb6 which means that the behavior of this particular electrode is mainly controlled by a diffusion process [30,31].

However, the T-GFD4.6 and T-GFA6 electrodes, show slope values greater than 0.5, thus suggesting a coupled diffusion and adsorption control. The main difference of these electrodes with T-AvCarb6 may be attributed to the less packed structures of the T-AvCarb6 fibers compared to the Sigracell ones. The greater slope values also confirm a pseudo-reversible redox reaction which is also observed by the slight deviation of ΔE from the 0.5 V value as the scan rates increase in the CV. The coupled diffusion and adsorption processes can shift the cathodic peaks towards more positive potential values as the scan rates increase. Further studies by EIS will confirm whether the irreversibility of the electrode reaction is due to a slow heterogeneous electron transfer or to a coupled homogeneous reaction.

To further evaluate the electrochemical response of the electrodes to the electron transfer effects, EIS tests were carried out to the T-GFD4.6, T-GFA6 and T-AvCarb6 electrodes. Fig. 9 shows the Nyquist plots obtained for the T-GFD4.6, T-AvCarb6 and T-GFA6 electrodes in 0.4 M $VOSO_4$ + 2 M H_2SO_4 electrolyte at 1.009 V vs Ag/AgCl. As can be observed, the Nyquist plots show similar responses for all the electrodes with an initial semicircle at high to medium frequencies, characteristic of a charge transfer mechanism. The T-GFD4.6 electrode showed the bigger semicircle, with a charge transfer resistance of 745 mΩ cm^2 which implies a high resistance to the charge transfer mechanism. The T-GFA6 and T-AvCarb6 electrodes showed lower charge transfer resistances, 18.9 mΩ cm^2 and 137 mΩ cm^2, respectively. The different semicircle size points to the fact that the thermal treatment influences the performance of the electrodes (wettability and active surface area) differently. The different nature of the graphite precursors, and the chemical composition after thermal treatment, affects the electrode performance. Thus, concerning the electrode performance in EIS experiments, it can be inferred that the Rayon-based electrode T-GFA6 is kinetically more reactive to the oxidation of VO^{2+}/VO_2^+ once the vanadium ions reach the graphite surface, followed by the T-AvCarb6 and the T-GFD4.6 electrodes. Tables S1 and S2 from the supporting information, show that the T-GFA6 electrode is the one that presents the lowest C=O/C—O ratio. So, the surface of this electrode is enriched in C—O compound which enhances the electrooxidation of the vanadium ions. This feature is also corroborated in the cyclic voltammograms of the electrode, with the highest current density values. Comparing the two electrodes with similar thicknesses, T-GFA and T-AvCarb6, the most striking aspect is the large semicircle developed by the T-AvCarb6 electrode at medium frequency. This corresponds, not only to the different precursor material of graphite, but also to an enriched surface chemistry and enhanced specific surface areas of T-GFA6. In this sense, the Nyquist plots for the T-GFD4.6 electrode shows an electrode with very high charge transfer resistance, which is consistent with the low specific surface area, compared to the T-GFA and T-AvCarb6 electrodes.

To gain insight on the effect of polarization cycles on electrode aging, the Nyquist plots of the Sigracell PAN electrode (GFD4.6-EA) after being polarized at 1.4 V vs Ag/AgCl are depicted in Fig. 10. As can be observed, all the plots show similar responses with an initial semicircle at high frequencies, characteristic of the charge transfer mechanism and

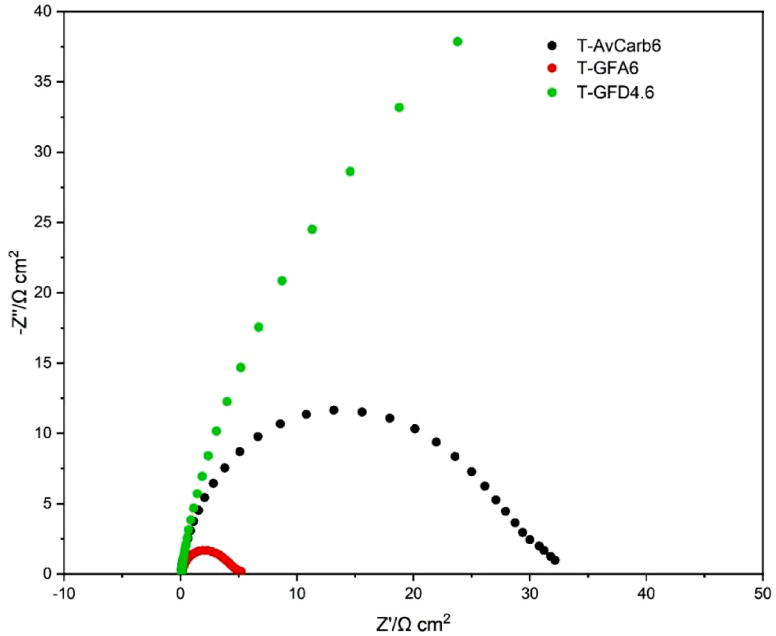

Fig. 9. Nyquist plots recorded for the T-GFD4.6, T-AvCarb6 and T-GFA electrodes in 0.4 M $VOSO_4$ + 2 M H_2SO_4 electrolyte at 1.009 V vs Ag/AgCl.

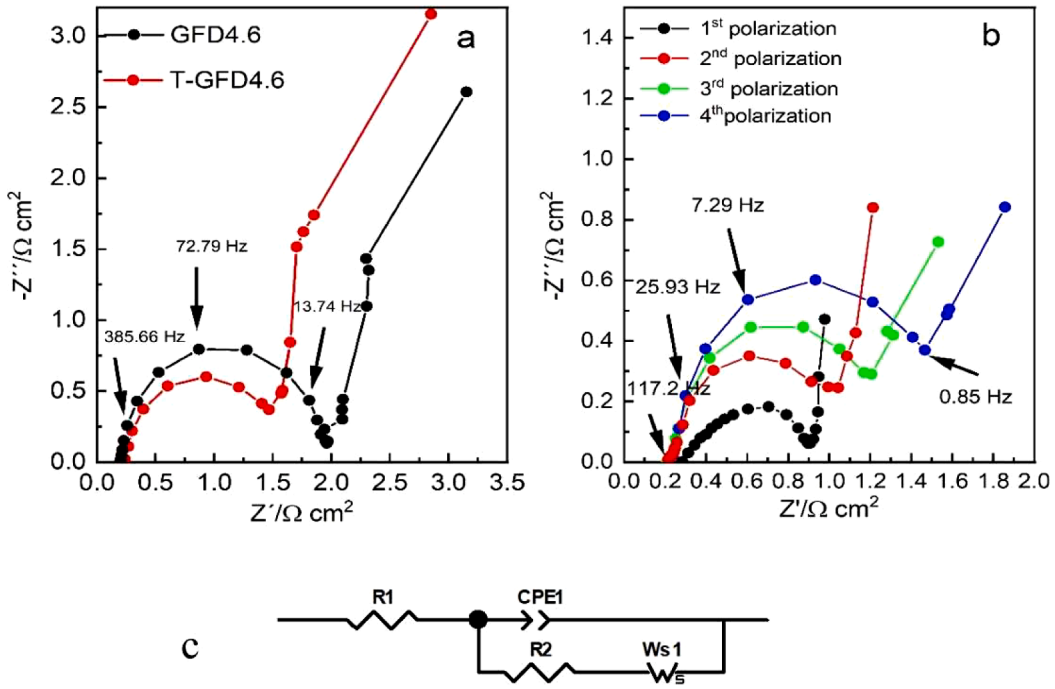

Fig. 10. (a) Nyquist plots of thermal treated and untreated GFD4.6-EA electrode, (b) T-GFD4.6 after a series of polarization cycles and (c) equivalent circuit.

a straight line at low frequencies that characterizes a mass transport mechanism (diffusion). Thus, this behavior indicates that the redox reaction of the VO^{2+}/VO_2^+ pair on this electrode is governed by two different mechanisms. The equivalent circuit of Fig. 10c), which fits the EIS data for the Nyquist plots of the T-GFD4.6 electrode (Fig. 10a), includes the contact resistance of the solution *R1*, a constant phase element, *CPE1*, which stands for the charge transfer resistance at the electrode-electrolyte interface *R2*, and the double layer capacitance (C_{dl}) of the faradic arc in the medium frequency region. Finally, the Warburg element *Ws1* describes the mass transport limited diffusion effect in the low frequency region.

As can be observed in Fig. 10b as the polarization tests evolve (counted as cycles of polarizations at 1.4 V and open circuit potential stabilization) the charge transfer resistance, *R2*, increases from 82.4 mΩ cm^2 to 142 mΩ cm^2, which might be attributed to a decrease in C=O functional groups of the thermally activated carbon felt T-GFD4.6 probably due to an oxidation process to CO_2. This implies a decrease of the wettability of the high porous carbon felt and less available oxygen compounds for the vanadium electrooxidation.

The Nyquist plots for the untreated electrode GFD4.6 before and after aging by polarization cycles in the vanadium solution are presented in Fig. 10a. The different semicircle sizes indicate that the thermal treatment influences the performance of the electrodes mainly due to modifications on their physical properties (wettability and active surface area) and chemical composition. The contact resistances of the solution *R1* for both electrodes are nearly the same, 20.5 mΩ cm^2 and 22.2 mΩ cm^2, respectively. However, the response to the charge transfer resistance of the faradic processes appears markedly modified. The activated carbon felt electrode shows a better performance to the potentiostatic polarization test than the untreated one. The treated electrode presents a charge transfer resistance, *R2*, of 141 mΩ cm^2 against 174.9 mΩ cm^2 for the untreated one. At low frequencies, both electrodes exhibit diffusion-limited behavior, typical of highly porous media.

4. Conclusions

In the present research, it has been demonstrated that thermal treatment of carbon felts can enhance their electrochemical performance towards oxidation of the VO^{2+}/VO_2^+ redox pair by the thermal modification of the graphite surface. Specifically, there is a gain in oxigenate compounds that enhances the electrode wettability and its performance. The surface modification of graphite felts can also be achieved electrochemically, which can also lead to improved oxidation processes from VO^{2+} to VO_2^+.

Different activation methods for the T-GFD4.6-EA thermally activated electrode have been developed in order reproduce an environment of cycling and continuous immersion in an oxidizing electrolyte, of a vanadium redox flow battery. Thus, despite having a catalytically active surface for vanadium oxidation, the chemical composition of the electrode surface changed differently depending on the test to which it was exposed. So, when exposed to the immersion in 2 M H_2SO_4 + 0.4 M $VOSO_4$ electrolyte the VO^{2+}/VO_2^+ oxidation reaction is favored, whereas aging after 100 cycles using the cyclic voltammetry technique increased it conductivity and the reversibility of the VO^{2+}/VO_2^+ redox reaction. This behavior can lead to suppose that when starting up an all-vanadium redox flow battery, GFD-type electrodes can chemically modify their surface until the electrode stabilizes, regardless of the prior thermal activation. There is still a lot of research to be developed, but it is expected that important results can be published in the future in this regard.

EIS analysis confirmed that the nature of the graphite precursors and the chemical composition after thermal treatment, affects the electrode wettability and performance. Accessibility of the electrolyte to the inner pores is crucial in order to avoid capacitive behavior, as observed for the T-GFD4.6 electrode compared to T-GFA6 and T-AvCarb6, at the high-medium frequency ranges. The thermal pretreatment was intended to stabilize the surface of the electrodes and prevent changes in their electrochemical behavior. However, the polarization of the electrodes in the acidic solution caused the modification of surface species, which led to the observed changes in electrochemical behavior towards VO^{2+}/VO_2^+ oxidation.

The results of this study suggest that thermally activated carbon felts may experience changes in their electrochemical performance during cycling in redox flow batteries. However, the stability of these electrodes is dependent on the precursor material and the thermal pretreatment to

which it has been subjected. Therefore, it is not possible to generalize these results to all electrodes. Further research is needed to determine the optimal electrode pretreatment for improving long-term electrochemical performance in corrosive media.

Despite all these results, different electrode treatments can have different results for different electrodes. It cannot be generalized, and a deep research should be performed to enhance long lasting electrochemical performance of these graphite felts in such corrosive media without any structural or surface chemistry modifications.

CRediT authorship contribution statement

José E. Barranco: Methodology, Investigation, Validation, Formal analysis, Writing – original draft. **Abdenbi Cherkaoui:** Investigation, Writing – review & editing. **Manuel Montiel:** Investigation, Conceptualization, Writing – review & editing, Funding acquisition. **Ana González-Espinosa:** Investigation, Writing – review & editing. **Antonio Lozano:** Writing – review & editing, Funding acquisition. **Félix Barreras:** Funding acquisition, Resources, Methodology, Writing – review & editing.

Declaration of Competing Interest

The authors declare the following financial interests/personal relationships which may be considered as potential competing interests: Felix Barreras reports financial support was provided by European Union. Felix Barreras reports financial support was provided by Spanish Ministry of Science and Innovation. Felix Barreras reports financial support was provided by Regional Government of Aragon.

Data availability

Data will be made available on request.

Acknowledgments

This research is part of the CSIC program for the Spanish Recovery, Transformation and Resilience Plan funded by the Recovery and Resilience Facility of the European Union, established by the Regulation (EU) 2020/2094. Support of the CSIC Interdisciplinary Thematic Platform (PTI+) Transición Energética Sostenible+ (PTI-TRANSENER+). Funding provided by the Spanish Ministry of Science and Innovation under project MAFALDA (PID2021–126001OB-C32), as well as the support of the Regional Government of Aragon to the Fuel Conversion Research Group (T06_23R).

Supplementary materials

Supplementary material associated with this article can be found, in the online version, at doi:10.1016/j.electacta.2023.143281.

References

[1] Energy Storage - 2021 - Ta - A comprehensive review of carbon-based and metal-based electrocatalysts in the vanadium redox.pdf, (n.d.).
[2] T.X. Huong Le, M. Bechelany, M. Cretin, Carbon felt based-electrodes for energy and environmental applications: a review, Carbon N Y 122 (2017) 564–591, https://doi.org/10.1016/j.carbon.2017.06.078.
[3] J.Z. Chen, W.Y. Liao, W.Y. Hsieh, C.C. Hsu, Y.S. Chen, All-vanadium redox flow batteries with graphite felt electrodes treated by atmospheric pressure plasma jets, J. Power Sources 274 (2015) 894–898, https://doi.org/10.1016/j.jpowsour.2014.10.097.
[4] I. Mustafa, A. Al Shehhi, A. Al Hammadi, R. Susantyoko, G. Palmisano, S. Almheiri, Effects of carbonaceous impurities on the electrochemical activity of multiwalled carbon nanotube electrodes for vanadium redox flow batteries, Carbon 131 (2018) 47–59, https://doi.org/10.1016/j.carbon.2018.01.069.
[5] L. Wei, T.S. Zhao, G. Zhao, L. An, L. Zeng, A high-performance carbon nanoparticle-decorated graphite felt electrode for vanadium redox flow batteries, Appl. Energy 176 (2016) 74–79, https://doi.org/10.1016/j.apenergy.2016.05.048.
[6] T. Liu, X. Li, H. Nie, C. Xu, H. Zhang, Investigation on the effect of catalyst on the electrochemical performance of carbon felt and graphite felt for vanadium flow batteries, J. Power Sources 286 (2015) 73–81, https://doi.org/10.1016/j.jpowsour.2015.03.148.
[7] W.H. Wang, X.D. Wang, Investigation of Ir-modified carbon felt as the positive electrode of an all-vanadium redox flow battery, Electrochim. Acta 52 (2007) 6755–6762, https://doi.org/10.1016/j.electacta.2007.04.121.
[8] X. Li, D. Fang, Y. Cao, Z. Luo, M. Jiang, W. Xu, C. Xiong, Template-sacrificed synthesis of polypyrrole nanofibers for lithium battery, J. Mater. Sci. 51 (2016) 9526–9533, https://doi.org/10.1007/s10853-016-0199-7.
[9] G. Milczarek, O. Inganäs, Renewable cathode materials from biopolymer/conjugated polymer interpenetrating networks, Science 335 (2012) 1468–1471, https://doi.org/10.1126/science.1215159.
[10] Q. Li, Q. Dong, T. Zhang, Z. Xue, J. Li, Z. Wang, H. Sun, Performance of room-temperature activated tubular polypyrrole modified graphite felt composite electrode in vanadium redox flow battery, Electrochim. Acta 409 (2022), 139970, https://doi.org/10.1016/j.electacta.2022.139970.
[11] L. Eifert, R. Banerjee, Z. Jusys, R. Zeis, Characterization of carbon felt electrodes for vanadium redox flow batteries: impact of treatment methods, J. Electrochem. Soc. 165 (2018) A2577–A2586, https://doi.org/10.1149/2.0531811jes.
[12] A. Kaur, K. Il Jeong, S. Su Kim, J. Woo Lim, Optimization of thermal treatment of carbon felt electrode based on the mechanical properties for high-efficiency vanadium redox flow batteries, Compos. Struct. 290 (2022), 115546, https://doi.org/10.1016/j.compstruct.2022.115546.
[13] A.M. Pezeshki, J.T. Clement, G.M. Veith, T.A. Zawodzinski, M.M. Mench, High performance electrodes in vanadium redox flow batteries through oxygen-enriched thermal activation, J. Power Sources 294 (2015) 333–338, https://doi.org/10.1016/j.jpowsour.2015.05.118.
[14] B. Sun, M. Skyllas-Kazacos, Modification of graphite electrode materials for vanadium redox flow battery application-I. Thermal Treatment, Electrochim. Acta (1992) 1253–1260, https://doi.org/10.1016/0013-4686(92)85064-R.
[15] S.P. Rigby, D. Barwick, R.S. Fletcher, S.N. Riley, Interpreting mercury porosimetry data for catalyst supports using semi-empirical alternatives to the Washburn equation, Appl. Catal. Gen. 238 (2003) 303–318, https://doi.org/10.1016/S0926-860X(02)00348-4.
[16] M. Gattrell, J. Park, B. MacDougall, J. Apte, S. McCarthy, C.W. Wu, Study of the mechanism of the vanadium 4+/5+ redox reaction in acidic solutions, J. Electrochem. Soc. 151 (2004) A123, https://doi.org/10.1149/1.1630594.
[17] M. Gattrell, J. Qian, C. Stewart, P. Graham, B. MacDougall, The electrochemical reduction of VO2+ in acidic solution at high overpotentials, Electrochim. Acta 51 (2005) 395–407, https://doi.org/10.1016/j.electacta.2005.05.001.
[18] I. Derr, D. Przyrembel, J. Schweer, A. Fetyan, J. Langner, J. Melke, M. Weinelt, C. Roth, Electroless chemical aging of carbon felt electrodes for the all-vanadium redox flow battery (VRFB) investigated by electrochemical impedance and X-ray photoelectron spectroscopy, Electrochim. Acta 246 (2017) 783–793, https://doi.org/10.1016/j.electacta.2017.06.050.
[19] Z. He, Y. Lv, T. Zhang, Y. Zhu, L. Dai, S. Yao, W. Zhu, L. Wang, Electrode materials for vanadium redox flow batteries: intrinsic treatment and introducing catalyst, Chem. Eng. J. 427 (2022), 131680, https://doi.org/10.1016/j.cej.2021.131680.
[20] P. Mazur, J. Mrlik, J. Pocedic, J. Vrana, J. Dundalek, J. Kosek, T. Bystron, Effect of graphite felt properties on the long-term durability of negative electrode in vanadium redox flow battery, J. Power Sources 414 (2019) 354–365, https://doi.org/10.1016/j.jpowsour.2019.01.019.
[21] Z. Wang, J. Ren, J. Sun, Z. Guo, L. Wei, X. Fan, T. Zhao, Characterizations and selections of electrodes with optimal performance for large-scale vanadium redox flow batteries through lab-scale experiments, J. Power Sources 549 (2022), 232094, https://doi.org/10.1016/j.jpowsour.2022.232094.
[22] D.J. Morgan, Comments on the XPS analysis of carbon materials, J. Carbon Res. 7 (2021) 51, https://doi.org/10.3390/c7030051.
[23] T.R. Gengenbach, G.H. Major, M.R. Linford, C.D. Easton, Practical guides for x-ray photoelectron spectroscopy (XPS): interpreting the carbon 1s spectrum, J. Vac. Sci. Technol. A 39 (2021), 013204, https://doi.org/10.1116/6.0000682.
[24] L.F. Chen, Z.H. Huang, H.W. Liang, Q.F. Guan, S.H. Yu, Bacterial-cellulose-derived carbon nanofiber@MnO2 and nitrogen-doped carbon nanofiber electrode materials: an asymmetric supercapacitor with high energy and power density, Adv. Mater. 25 (2013) 4746–4752, https://doi.org/10.1002/adma.201204949.
[25] R. Pietrzak, XPS study and physico-chemical properties of nitrogen-enriched microporous activated carbon from high volatile bituminous coal, Fuel 88 (2009) 1871–1877, https://doi.org/10.1016/j.fuel.2009.04.017.
[26] H.J. Lee, H. Kim, Graphite felt coated with dopamine-derived nitrogen-doped carbon as a positive electrode for a vanadium redox flow battery, J. Electrochem. Soc. 162 (2015) A1675–A1681, https://doi.org/10.1149/2.0081509jes.
[27] W. Zhang, J. Xi, Z. Li, H. Zhou, L. Liu, Z. Wu, X. Qiu, Electrochemical activation of graphite felt electrode for VO2+/VO2+ redox couple application, Electrochim. Acta 89 (2013) 429–435, https://doi.org/10.1016/j.electacta.2012.11.072.
[28] M. Taş, P.J. Alphonse, İ. Kayali, G. Elden, Comparison of commertial electrodes in terms of mass and charge transports in a of vanadium redox flow battery, International Symposium on Electric Aviation and Autonomous Systems (ISEAS) (2020).

[29] J. Lawton, S. Tiano, D. Donnelly, S. Flanagan, T. Arruda, The effect of sulfuric acid concentration on the physical and electrochemical properties of vanadyl solutions, Batteries 4 (2018) 40, https://doi.org/10.3390/batteries4030040.

[30] K. Suliborska, M. Baranowska, A. Bartoszek, W. Chrzanowski, J. Namieśnik, Determination of antioxidant activity of vitamin C by voltammetric methods, Proceedings 11 (2019) 23, https://doi.org/10.3390/proceedings2019011023.

[31] A.J. Bard, L.R. Faulkner, Electrochemical Methods: Fundamentals and Applications, 2nd ed, Wiley, New York, 2001.